Crystallographic and Electronic Structure of Self-Assembled DIP Monolayers on Au(111) Substrates

ARTICLE *in* THE JOURNAL OF PHYSICAL CHEMISTRY C · MARCH 2008

Impact Factor: 4.77 · DOI: 10.1021/jp800631p · Source: OAI

Crystallographic and Electronic Structure of Self-Assembled DIP Monolayers on Au(111) Substrates

Dimas G. de Oteyza,*,†,‡,§ Esther Barrena,‡,§,|| Miguel Ruiz-Osés,† Iñaki Silanes,† Bryan P. Doyle,⊥ J. Enrique Ortega,†,#,^ Andrés Arnau,†,#,+ Helmut Dosch,Δ,§ and Yutaka Wakayama‡

Donostia International Physics Center, Paseo Manuel Lardizabal 4, 20018 San Sebastián, Spain, Advanced Electronic Materials Center, National Institute for Materials Science, 1-1 Namiki, Tsukuba 305-0044, Japan, Max-Planck-Institut für Metallforschung, Heisenbergstr. 3, 70569 Stuttgart, Germany, International Centre for Young Scientists, National Institute for Materials Science, 1-1 Namiki, Tsukuba 305-0044, Japan, Laboratorio Nazionale TASC, INFM-CNR, Area Science Park, I-34012 Basovizza, Trieste, Italy, Unidad Fisica de Materiales, Centro Mixto CSIC-UPV/EHU, Paseo Manuel Lardizabal 3, 20018 San Sebastián, Spain, Departamento de Fisica Aplicada UPV/EHU, Plaza de Oñate 2, 20018 San Sebastián, Spain, Departamento Fisica de Materiales UPV/EHU, Apdo. 1072, San Sebastián, Spain, and Institut für Theoretische und Angewandte Physik, Universität Stuttgart, 70550 Stuttgart, Germany

Received: January 22, 2008; In Final Form: February 26, 2008

We report a comprehensive study of the self-assembly of a diindenoperylene (DIP) monolayer on Au(111) single crystals exploiting different electron probes ranging from STM and LEED to photoelectron spectroscopy and NEXAFS. By this multitechnique approach, we obtain a full picture of the crystallographic and electronic structure of the DIP layer as well as an insight into the assembly process and the role of the DIP−Au interactions. We contrast these experimental findings with theoretical calculations.

Introduction

The development of organic electronics into an industrially competing technology still faces big challenges intimately related to device performance and to further miniaturization. The performance drawback can be alleviated by optimization of the organic film structure and morphology,[1−3] whereas further miniaturization requires improved bottom-up design strategies. In this respect, self-assembly of organic semiconducting molecules is considered one of the most promising routes toward success.[4−6] Therefore, many efforts are currently devoted to improving our microscopic understanding of organic self-assembly on technologically relevant substrates, which might eventually allow molecular control of the resulting structures and morphologies.

Diindenoperylene (DIP) has proven to be a highly interesting molecule because of its ambipolar behavior.[7] Various growth studies have evidenced exceptional order of DIP films, which is one of the requirements for high charge carrier mobilities.[8,9] Measurements on operating devices have shown the contact resistance to often be the main bottleneck for charge transport, emphasizing the importance of the first layers at organic−metal interfaces in device performance, since they define the charge carrier injection into the active semiconducting films.[10,11] However, structural studies on the first DIP layers have only been carried out on SiO_2 substrates.[12,13] On relevant organic−metal interfaces, such as DIP/Au, previous characterizations dealt with films of hundreds of nm.[14] Here we report a study of the first DIP monolayer on top of Au(111) single crystals, in which the growth and the crystallographic and the electronic structure are characterized by a multitechnique approach, comprising scanning tunneling microscopy (STM), low-energy electron diffraction (LEED), photoelectron spectroscopy, and near edge X-ray absorption fine structure (NEXAFS) spectroscopy, and are critically compared with theoretical predictions.

Experimental and Theoretical Methods

The STM characterization was performed in constant current mode in a commercial JEOL UHV system,[15] including two interconnected growth and measurement chambers (each with base pressures of 10^{-10} mbar). The Au(111) substrate was prepared by repeated Ar sputtering ($E = 600$ eV) and annealing cycles ($T \sim 520$ °C) until clean surfaces with large terraces exhibiting the well-known $(22\times\sqrt{3})$ Au(111) surface reconstruction (also referred as herringbone reconstruction) could be observed. The DIP molecules, purified twice by gradient sublimation before use, were subsequently evaporated from a Knudsen cell with a deposition rate of approximately 0.1 monolayer (ML) per minute.

The LEED, photoelectron, and NEXAFS spectroscopy measurements were carried out at the UE56/2-PGM1 beamline at the BESSY Synchrotron in Berlin which is equipped with a SPECS 100 high-resolution angle-resolved hemispherical analyzer. For the photoelectron spectroscopy experiments, the pass energy was set to 20 eV. The excitation energies were 62 and

* To whom correspondence should be addressed. E-mail: d_g_oteyza@ehu.es. Current address: Donostia International Physics Center. Tel.: +34 943015389. Fax: +34 943015600.
† Donostia International Physics Center.
‡ Advanced Electronic Materials Center, National Institute for Materials Science.
§ Max-Planck-Institut für Metallforschung.
|| International Centre for Young Scientists, National Institute for Materials Science.
⊥ INFM-CNR.
Unidad Fisica de Materiales.
^ Departamento de Fisica Aplicada UPV/EHU.
+ Departamento Fisica de Materiales UPV/EHU.
Δ Universität Stuttgart.

10.1021/jp800631p CCC: $40.75
Published on Web 03/18/2008

330 eV for the valence band and the C 1s core-level photoelectron spectroscopy measurements, respectively. The pass energy for the NEXAFS experiments was 100 eV, which were recorded in Auger yield mode (set to a kinetic energy of 260 eV). The spectra were normalized with those obtained from the clean Au(111) surface. The substrate was prepared as in the STM experiments by sputter-anneal cycles, and its cleanliness was checked requiring that no C signal was found by XPS, that the surface state was visible by angle-resolved valence band photoelectron spectroscopy, and that the LEED pattern evidenced the herringbone superstructure.

The theoretical calculations were carried out with the SIESTA code[16] which is based on DFT calculations with the Perdew-Burke-Ernzerhof functional, a double-Z plus polarization basis set, a 100 meV energy shift, and a 300 Ry mesh cutoff for the spatial grid. The Au(111) surface was not included in the calculations.

Results and Discussion

The formation of the DIP monolayer was monitored by STM at different stages of its growth at room temperature. Figure 1a corresponds to an image with submonolayer coverage (0.5 ML) and depicts various important points with respect to the film growth. The adsorbed DIP molecules are highly mobile on the Au surface. Thus, the very first stages of the film formation result in a 2D gas of mobile molecules even at substrate temperatures down to at least 150 K. This is evidence of the low molecule−substrate interaction.[17−19] Note, however, that the molecules are finally immobilized at specific nucleation sites, such as the step edges (highlighted in a zoom in Figure 1a) and the "elbows" of the herringbone reconstruction (highlighted with arrows and a zoom in Figure 1a). The fact that the molecules appear "engraved" instead of as protrusions on the substrate surface is related to the previously mentioned 2D gas covering the surface and surrounding the stabilized molecules. The preferred nucleation of organic overlayers modulated by surface reconstruction patterns or step edges has already been observed in previous studies and has even been exploited for the controlled synthesis of nanostructured systems.[20−28]

The DIP molecules adsorbed at the step edges align their long molecular axis parallel to the step direction and consequently form rows in a head-to-tail configuration. In contrast, the adsorption at the reconstruction elbows does not give clear evidence of any preferred molecular orientation. Upon further growth of the nuclei, no order is developed among the molecules. This is a signature of the low intermolecular interactions, as expected from the absence of functional groups with the potential to form H-bonds or give rise to any other interactions stronger than the van der Waals contribution. Only in large DIP assemblies extending over more than 100 nm^2 do we find a long range ordered structure. A discrete number of rotational domains is observed, evidencing the role of the substrate as template directing the molecular ordering. Interestingly, the different domains are not separated by abrupt boundaries but often follow a gradual transition among the different orientations. This can be observed in Figure 1a (which shows three different domains) between the domains numbered #2 and #3. This is the product of weak and smooth interaction potentials (both molecule-substrate and molecule−molecule) in these organic systems, which allow a much higher accommodation of strain than is generally known from inorganic materials.[1,2] The reconstruction of the underlying Au(111) surface remains visible below the DIP layer, which is a consequence of the weak molecule−substrate interaction. In other words, the molecule−substrate interactions (van der Waals) are on the one hand too weak to affect the Au(111) surface reconstruction but, on the other hand, strong enough to dictate the epitaxial growth of the organic overlayer. Nevertheless, the observation that many of the borders of these DIP assemblies follow the corrugation lines of the herringbone reconstruction (as shown for example by two dashed lines in Figure 1a) reveals a non-negligible energetic barrier for the growth processes (i.e., diffusion or incorporation onto the 2D molecular crystal sites) across these lines.

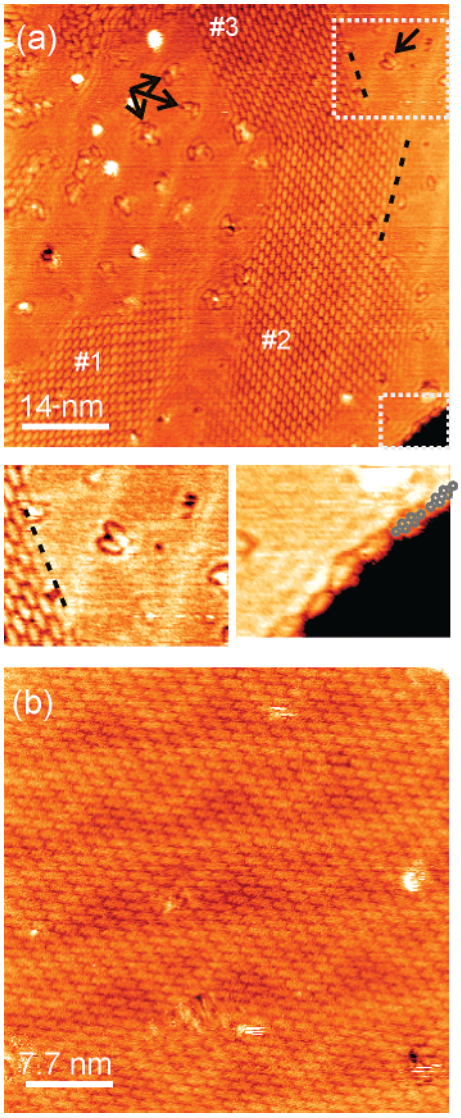

Figure 1. Constant current STM images taken at room temperature of a DIP film after (a) 0.5 ML coverage ($V = 1.9$ V, $I = 50$ pA) and (b) 1 ML ($V = -1$ V, $I = 80$ pA) coverage. The arrows in panel a mark, by way of example, the adsorption of DIP molecules at the elbows of the Au herringbone reconstruction, the dotted lines mark some of the domain limits following the corrugation lines, and the numbers correspond to each of the three different domains observed in the image. The images below correspond to zooms taken as marked on the image, to highlight the role of the step edges, the herringbone reconstruction and its elbows. Two molecules are schematically overlaid on the right zoom to clarify the molecular orientation.

Close to completion of the first monolayer, a well ordered film (see Figure 1b) with ordered domains extending over up to more than 100 nm forms. The epitaxial relation between the ordered DIP and the Au substrate has been carefully examined from numerous STM images exhibiting different domains and from the LEED pattern obtained from a complete DIP monolayer (Figure 2a). In the following, we will call the high-

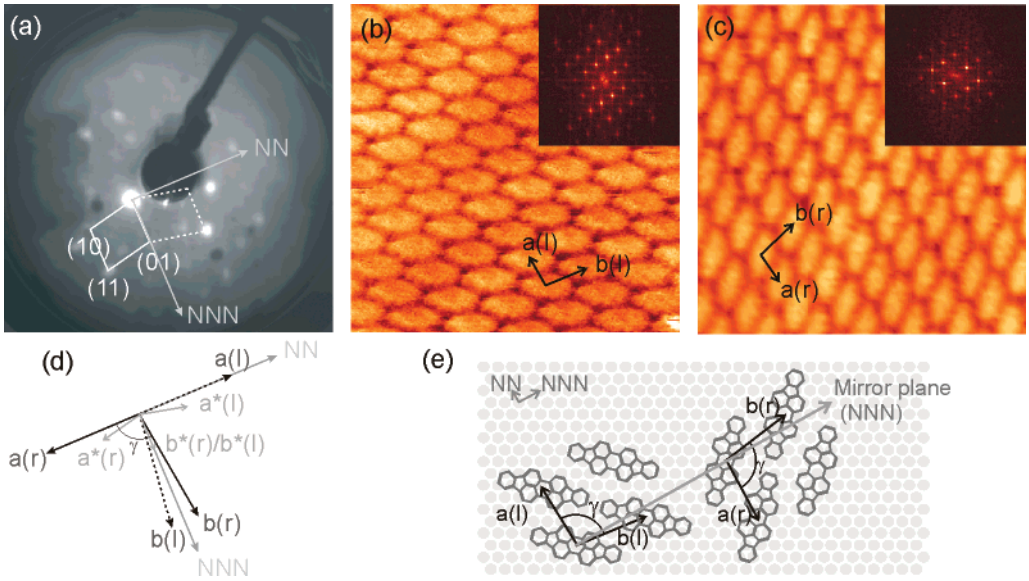

Figure 2. (a) LEED pattern obtained on a 1 ML DIP film on Au(111) at 15 eV. The NN and NNN Au directions are marked as obtained from measurement of the Au diffraction spots. One of the reciprocal unit cells of the corresponding DIP film structure is overlaid on the image by the solid line (its enantiomorphic domain is plotted with a dotted line). The reflections included in this cell are indexed accordingly. (b and c) 12 × 12 nm^2 constant current STM images (the corresponding FFT images in the insets) revealing the film structure of left-handed (b) and right-handed (c) enantiomorphic domains. The unit cell vectors are superimposed on the images. (d) Correspondence between the reciprocal unit cells shown in (a) and the real space unit cells, together with the substrate high-symmetry directions. (e) Model of the unit cell and molecular orientations for the two enantiomorphic domains of panels b and c, in relation to the underlying hexagonal Au surface. Neither the error bars in each of the parameters, nor the herringbone reconstruction, nor translational aspects with respect to the Au surface, are accounted for in this simplified scheme.

symmetry directions of the Au(111) hexagonal surface structure the nearest neighbor (NN) and next nearest neighbor (NNN) directions, corresponding to the [−110] and [−211] directions (and those related by the hexagonal symmetry), respectively. The diffraction peaks obtained from the DIP monolayer, which represent lattice points of the reciprocal film structure, can all be accurately accounted for by two enantiomorphic domains (with right- and left-handed coordinate systems, respectively) and their three corresponding rotational domains related by hexagonal substrate symmetry. The monolayer thus comprises a total of six equivalent DIP domains. One of the right-handed reciprocal unit cells is overlaid on the LEED image (solid line in Figure 2a), and the diffraction spots within the cell are indexed accordingly. The left-handed enantiomorphic domain, resulting from the mirror symmetry along the NNN direction (independently determined from the Au(111) LEED spots), is shown by the dashed line. The correspondence between these two reciprocal cells and their related real space unit cells is depicted in Figure 2d. All domains were also observed by STM. Panels b and c in Figure 2 depict high-resolution STM images corresponding to one of the left-handed domains (b) and its enantiomorphic right-handed domain (c). The LEED and STM results are self-consistent and give $a = 13.4 \pm 1$ Å, $b = 14.8 \pm 1$ Å, and $\gamma = 97 \pm 2°$ for parameters of the primitive unit cell. The a vector is directed along the NN directions of the Au substrate, which evidence a point-on-line type of epitaxy.[29]

The DIP molecule is directed almost along the unit cell diagonal, so that the monolayer consists of rows of virtually collinear molecules (Figure 2, panels b and c).[30] Figure 2e illustrates unit cells similar to those outlined in panels b and c of Figure 2, placed in relation to the hexagonal substrate lattice. The molecular axis appears 15 ± 3° deviated from the high-symmetry substrate directions. Periodic boundary contiditions (PBC) calculations were carried out on a planar array of DIP molecules. We used the experimental cell vectors as a starting point, and optimized them to minimum energy with the Nelder−Mead simplex algorithm.[31] The resulting theoretical parameters

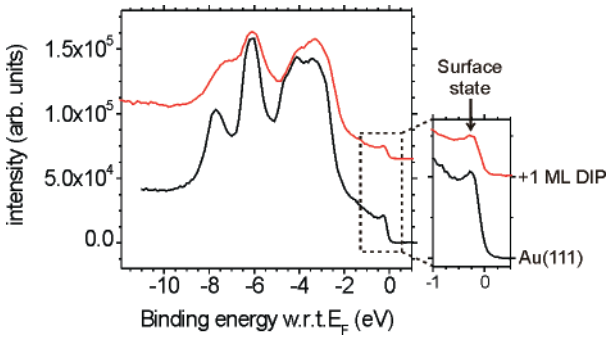

Figure 3. Normal emission valence band photoelectron spectroscopy data of the clean Au(111) surface (bottom) and of 1 ML DIP on Au(111) (top). The inset shows a magnification of the surface state region.

were $a = 12.41$ A, $b = 13.47$ A, and $\gamma = 96.5°$. In spite of the neglected substrate influence (except for the planarity requirement), the agreement with the experimental values is rather striking, further evidencing the weak DIP−Au(111) interactions. The calculated intermolecular binding energy is very low (51 meV), as expected for weak van der Waals contributions. Thus, steric effects and an optimized packing geometry seem to be among the main factors controlling the self-assembly of DIP monolayers on Au(111).

The electronic structure of the system has been investigated by photoelectron and NEXAFS spectroscopy experiments. The valence band normal emission spectra recorded before and after deposition of 1 ML of DIP on the clean Au(111) surface are shown in Figure 3. The spectra are dominated by the high intensity of the Au 5d levels, which prevent the proper observation of the occupied molecular orbitals. Due to the weak molecule−substrate interaction, the Au surface-state peak persists close to the Fermi level. It is in perfect accordance with the observation of the herringbone reconstruction underneath the DIP layer. Similar findings have been observed for other weakly interacting molecules such as PTCDA, NTCDI, or

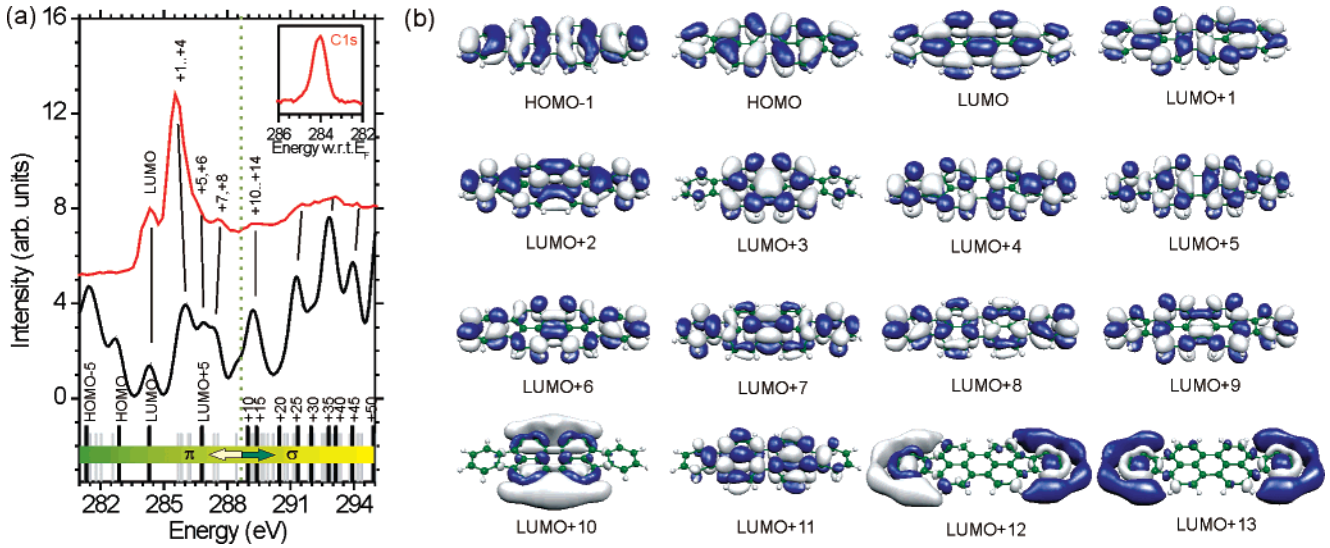

Figure 4. (a) Top: C K-edge NEXAFS spectrum and C 1s core-level spectrum (inset) of 1 ML DIP on Au(111). Bottom: Calculated density of states, result of a convolution of Gaussian peaks of 0.4 eV width, centered at each of the electronic levels marked (and indexed) by straight lines on the bottom axis. The energy scale of the eigenvalues has been shifted to match theory and experiment at the LUMO peak. The lines evidence the reasonably good correspondence of the main experimental spectral features with the calculations. (b) Calculated density distribution of different molecular levels. The main π or σ character of the orbitals is observed for those levels closer to or further from the Fermi energy, respectively.

BDG.[20,26,32−34] According to previous measurements on a wider range of DIP film thicknesses, the HOMO position is at a binding energy of ~1 eV with respect to E_F.[14] This and the following HOMO levels, however, remained inaccessible in our experiment. The reasons remain unclear, but might be explained by the different experimental setup, i.e., an excitation energy of 62 vs 22 eV, or by inhomogeneities in the angle-dependence of the photoelectron spectroscopy, given our angle-resolved data (but limited in this experiment to the Γ direction) as opposed to the integrated intensity in ref 14.

The C 1s core-level photoelectron spectroscopy spectra measured on the DIP films disclose one single peak with a width of 0.7 eV and a binding energy with respect to the Au Fermi level of 284.1 eV (inset in Figure 4a). Together with DFT calculations on the molecular electronic structure, this single initial level allows the identification of the empty molecular orbitals (LUMO levels) probed by NEXAFS at the C K-edge and shown in Figure 4a. The theoretical density of states (below the experimental spectrum) corresponds to the convolution of Gaussian curves of 0.4 eV width at each of the obtained molecular levels (marked by straight lines on the lower axis). The spatial charge distribution of the empty levels is shown in Figure 4b. The energy scale of the eigenvalues is defined to match the experimental data at the LUMO level. The main features in the experimental spectrum can then easily be identified. However, the proximity of various unoccupied levels makes them indistinguishable by NEXAFS measurements. Thus, while the LUMO is clearly identified, the consequent large peak corresponds to overlapping contributions from the LUMO+1, +2, +3, and +4 levels.

The correspondence between successive features in the experimental spectrum and the theoretical levels is outlined in Figure 4a. The calculations are extended to occupied HOMO levels that cannot be probed in NEXAFS. We can thus determine a HOMO−LUMO gap of 1.44 eV, in good agreement with previous calculations.[35] The spatial charge distribution in Figure 4b allows one to assign π^* or σ^* character in the orbital series. The main π character can be observed for the lowest energy orbitals, which then changes to a dominating σ character for the orbitals above the LUMO+9 level. This is also outlined in Figure 4a, in which the dotted vertical line represents the edge where the general orbital character changes from π to σ.

Conclusions

By complementary experimental techniques and theoretical calculations, we obtain a full picture of the crystallographic and electronic structure of the first DIP monolayer on a Au(111) surface, as well as insight into the assembly process and the role of the DIP−Au interactions. The DIP adsorbs with its molecular plane parallel to the substrate surface, favoring as adsorption sites step edges and the kinks of the herringbone reconstruction. Further growth finally leads to well ordered films with extended domains and a clear epitaxial relation with the substrate, in spite of the weak molecule−substrate interaction concluded from various independent measurements. Additional DFT calculations disclose the electronic structure of the molecules, in good agreement with the experimental spectroscopy data associated to the organic film.

Acknowledgment. We thank P. M. Schmidt-Weber, T. Kampen, and S. Mähl for technical support during the beamtime in BESSY. We thank J. Pflaum and S. Hirschmann for purification of the molecules. This work was supported by the European Community − Research Infrastructure Action under the FP6 "Structuring the European Research Area" Programme (through the Integrated Infrastructure Initiative "Integrating Activity on Synchroton and Free Electron Laser Science -Contract R II 3-CT-2004-506008"). The work was further supported through projects of the University of the Basque Country (GIU06/27) and the Spanish Ministerio de Educacion y Ciencia (MAT2007-63083). I.S. and A.A. thank UPV/EHU (Grant IT-366-07) and MEC (Grant FIS2007-66711-C02-01) for partial financial support.

References and Notes

(1) Witte, G.; Wöll, C. *J. Mater. Res.* **2004**, *19*, 1889.
(2) Forrest, S. R. *Chem. Rev.* **1997**, *97*, 1793.
(3) Forrest, S. R. *Nature* **2004**, *428*, 911.
(4) Hecht, S. *Angew. Chem. Int. Ed.* **2003**, *42*, 24.
(5) De Feyter, S.; De Schryver, F. C. *Chem. Soc. Rev.* **2003**, *32*, 139.
(6) Barth, J. V.; Costantini, G.; Kern, K. *Nature* **2005**, *437*, 671.

(7) Tripathi, A. K.; Pflaum, J. *Appl. Phys. Lett*. **2006**, *89*, 082103.

(8) Dürr, A. C.; Schreiber, F.; Munch, M.; Karl, N.; Krause, B.; Kruppa, V.; Dosch, H. *Appl. Phys. Lett.* **2002**, *81*, 2276.

(9) Dürr, A. C.; Schreiber, F.; Ritley, K. A.; Kruppa, V.; Krug, J.; Dosch, H.; Struth, B. *Phys. Rev. Lett*. **2003**, *90*, 016104.

(10) Puntambekar, K. P.; Pesavento, P. V.; Frisbie, C. D. *Appl. Phys. Lett*. **2003**, *83*, 5539.

(11) Nichols, J. A.; Gundlach, D. J.; Jackson, T. N. *Appl. Phys. Lett*. **2003**, *83*, 2366.

(12) Zhang, X. N.; Barrena, E.; de Oteyza, D. G.; Dosch, H. *Surf. Sci*. **2007**, *601*, 2420.

(13) Kowarik, S.; Gerlach, A.; Sellner, S.; Schreiber, F.; Cavalcanti, L.; Konovalov, O. *Phys. Rev. Lett*. **2006**, *96*, 125504.

(14) Dürr, A. C.; Koch, N.; Kelsch, M.; Rühm, A.; Ghijsen, J.; Johnson, R. L.; Pireaux, J.-J.; Schwartz, J.; Schreiber, F.; Dosch, H.; Kahn, A. *Phys. Rev. B* **2003**, *68*, 115428.

(15) The image processing and data analysis was performed with the software WSxM. See: Horcas, I.; Fernandez, R.; Gomez-Rodriguez, J. M.; Colchero, J.; Gomez-Herrero, J.; Baro, A. M. *Rev. Sci. Instum*. **2007**, *78*, 013705.

(16) Soler, J. M.; Artacho, E.; Gale, J. D.; García, A.; Junquera, J.; Ordejón, P.; Sánchez-Portal, D. *J. Phys.: Condens. Matter* **2002**, *14*, 2745.

(17) Xu, B.; Tao, C.; Williams, E. D.; Reutt-Robey, J. E. *J. Am. Chem. Soc*. **2006**, *128*, 8493.

(18) Berner, S.; Brunner, M.; Ramoino, L.; Suzuki, H.; Güntherodt, H.-J.; Jung, T. A. *Chem. Phys. Lett*. **2001**, *348*, 175.

(19) Barrena, E.; de Oteyza, D. G.; Dosch, H.; Wakayama, Y. *ChemPhysChem* **2007**, *8*, 1915.

(20) Mendez, J.; Caillard, R.; Otero, G.; Nicoara, N.; Martin-Gago, J. A. *Adv. Mater*. **2006**, *18*, 2048.

(21) Fernandez-Torrente, I.; Monturet, S.; Franke, K. J.; Fraxedas, J.; Lorente, N.; Pascual, J. I. *Phys. Rev. Lett*. **2007**, *99*, 176103.

(22) Lin, J.-L.; Rausher, H.; Kirakosian, A.; Himpsel, F. J.; Dowben, P. A. *J. Appl. Phys.* **1999**, *86*, 5492.

(23) Rauscher, H.; Jung, T. A.; Lin, J.-L.; Kirakosian, A.; Himpsel, F. J.; Rohr, U.; Müllen, K. *Chem. Phys. Lett.* **1999**, *303*, 363.

(24) Yokoyama, T.; Yokoyama, S.; Kamikado, T.; Okuno, Y.; Mashiko, S. *Nature* **2001**, *413*, 619.

(25) Cañas-Ventura, M. E.; Xiao, W.; Wasserfallen, D.; Müllen, K.; Brune, H.; Barth, J. V.; Fasel, R. *Angew. Chem. Int. Ed*. **2007**, *46*, 1814.

(26) Ruiz-Osés, M.; Gonzalez-Lakunza, N.; Silanes, I.; Gourdon, A.; Arnau, A.; Ortega, J. E. *J. Phys. Chem. B* **2006**, *110*, 25573.

(27) Schiller, F.; Ruiz-Osés, M.; Ortega, J. E.; Segovia, P.; Martinez-Blanco, J.; Doyle, B. P.; Pérez-Dieste, V.; Lobo, J.; Néel, N.; Berndt, R.; Kröger, J. *J. Chem. Phys*. **2006**, *125*, 144719.

(28) Wakayama, Y. *J. Phys. Chem. C* **2007**, *111*, 2675.

(29) Hooks, D. E.; Fritz, T.; Ward, M. D. *Adv. Mater*. **2001**, *13*, 227.

(30) The most intense diffraction spots, i.e., the six (11) reflections, correspond to the diffraction by adjacent DIP rows. Their stronger intensity is related to the highly anisotropic molecular structure factor of these organic molecules, whose magnitude decay vs momentum transfer is much slower along the shorter molecular axis than along the longer one (see: de Oteyza, D. G.; Barrena, E.; Ossó, J. O.; Sellner, S.; Dosch, H. *J. Am. Chem Soc*. **2006**, *128*, 15052).

(31) Nelder, J. A.; Mead, R. *Comput. J.* **1965**, *7*, 308.

(32) Schmitz-Hübsch, T.; Fritz, T.; Sellam, F.; Staub, R.; Leo, K. *Phys. Rev. B* **1997**, *55*, 7972.

(33) Kilian, L.; Umbach, E.; Sokolowski, M. *Surf. Sci*. **2006**, *600*, 2633.

(34) Ruiz-Osés, M.; Kampen, T.; González-Lakunza, N.; Silanes, I.; Schmidt-Weber, P. M.; Gourdon, A.; Arnau, A.; Horn, K.; Ortega, J. E. *ChemPhysChem* **2007**, *8*, 1722.

(35) Ramaniah, L. M.; Boero, M. *Phys. Rev. A* **2006**, *74*, 042505.